Surface Science

Chemical and Elemental Analysis

Correction of non-linearity in detectors for electron spectroscopy
Mannella, N., S. Marchesini, S.-H. Yang, B.S. Mun, A.W. Kay, T. Gresch, A. Rosenhahn, C.S. Fadley

Development of a GHz-rate detector for synchrotron radiation research
Turko, B., M. Press, A.W. Kay, M. West, J.E. Katz, H. Spieler, Z. Hussain, C.S. Fadley, B. Ludewigt, J.-M. Bussat, P. Denes, H. von der Lippe, G. Meddler, G. Zizka, G. Lebedev, M. Mellon, T. Wiell

High resolution XPS investigation of oxide layer growth on Ge substrates
Tabet, N., M. Faiz, N. Hamdan, Z. Hussain

Optimization of PEEM-2 for studies of organic thin film
Morin, C., A.P. Hitchcock, H. Ikeura-Sekiguchi, A. Scholl, A. Doran, K. Kaznacheyev

Soft x-ray emission spectroscopy of the liquid-solid interface between water and a Cu(In,Ga)(S,Se)$_2$ thin film solar cell absorber
Heske, C., U. Groh, O. Fuchs, L. Weinhardt, E. Umbach, Ch.-H. Fischer, Th. Schedel-Niedrig, M.Ch. Lux-Steiner, S. Zweigart, F. Karg, J.D. Denlinger, B. Rude, C. Andrus, F. Powell

Use of synchrotron reflectance infrared spectromicroscopy as a rapid, direct, non-destructive method for the study of inks on paper
Wilkinson, T.J., D.L. Perry, M.C. Martin, W.R. McKinney, A.A. Cantu

X-ray magnetic linear dichroism of Fe-Ni alloys on Cu(111)
Johnson, T.F., Y. Sato, S. Chiang, M. Hochstrasser, J.G. Tobin, J.A. Giacomo, J.D. Shine, X.D. Zhu, D.P. Land, D.A. Arena, S.A. Morton, G.D. Waddill

Correction of Non-Linearity in Detectors for Electron Spectroscopy

N. Mannella[1,2], S. Marchesini[2], S.-H. Yang[2], B.S. Mun[1,2], A.W. Kay[1,2,#], T. Gresch[2,3], A. Rosenhahn[2] and C.S. Fadley[1,2]

[1]Dept. of Physics, University of California-Davis, Davis, CA 95616
[2]Materials Sciences Division, Lawrence Berkeley National Laboratory, Berkeley, CA 94720
[3]Institute of Physics, University of Zurich, Zurich, Switzerland
[#]Present address: Intel Corporation, Portland, OR

INTRODUCTION

The intensity levels reached in many third-generation synchrotron radiation experiments on solids have been found to exceed the linear response range of the final detection system involved. In electron spectroscopy, Seah and co-workers have previously discussed methods for detecting such non-linearity, including measurements with laboratory x-ray sources [1]. As a particular case involving synchrotron radiation, non-linearity has been noticed by several groups in using the Gammadata/Scienta electron spectrometers, with this behavior extending even to fairly low countrates [2-8]. For example, prior work on multi-atom resonant photoemission (MARPE) by several groups was strongly affected by this particular non-linearity [3-6]. While data related to the MARPE effect have been corrected for such non-linearities in prior publications [6b,7,8], we have found that other measurements such as the quantitative analysis of complex oxides via core-level intensities can be strongly influenced by this non-linearity, even when the exciting energy is far away from any resonance [9]. Similarly, measurements of relative intensities in angle-resolved valence spectra can also be significantly altered [10]. It is thus of interest to develop accurate and broadly utilizable procedures for correcting for non-linearity with any detection system. Although we will use one spectrometer system as an example, the methodologies discussed here should be useful for many other cases.

CORRECTION METHODOLOGIES AND EXPERIMENTAL RESULTS

In Figure 1(a), we show broad-range survey spectra from a Cu(110) sample, as excited by Al Kα radiation with various power levels and detected by a Scienta SES200 spectrometer and its standard microchannel-plate/phosphor/CCD detection system. Since the high voltage was held constant, this is verified experimentally to lead to x-ray flux being proportional to power [7]. The various spectra have been normalized to one another at the lowest-countrates, just above the valence region. If the detector were linear, all spectra should lie on top of one another, but it is evident that they are not, with factors of up to 4x separating them in the higher intensity regions at lower kinetic energy.

We now consider two methods for correcting for non-linearity in such spectra:

1. Measurement of flat-background reference intensity as a function of incident x-ray flux: In the most obvious method, a flat background region in a spectrum from a sample with a stable surface can simply be measured as a function of incident x-ray flux, with non-linearity then being reflected in any deviation of a plot of measured intensity vs. x-ray flux from a straight line [7]. One might term this a "partial yield" measurement of detector response. This curve can then be fit to a convenient polynomial function such that any non-linearity can be described finally via:

$$I_m(I_t, I_x) = b_0 + b_1 I_t(I_x) + \sum_{n=2}^{n_{max}} b_n I_t(I_x), \tag{1}$$

where I_m = the measured countrate, I_t = the true countrate, I_x = the incident x-ray flux, the b_n are empirical expansion coefficients, and n_{max} is some maximum order chosen to adequately fit the data (roughly 5 in one prior analysis [7]). The coefficient b_0 thus represents the dark current in the absence of any excitation, and this will often be negligible, or at least can be simply subtracted from all measurements. The overall counting efficiency ε is now defined simply as

$$\varepsilon(I_m) = \frac{I_m(I_t, I_x) - b_0}{I_t(I_x)} = b_1 + \sum_{n=2}^{n_{max}} b_n I_t^{n-1}(I_x). \tag{2}$$

Actual measured spectra can now be generally written as vectors $[I_{mi}(E_i)]$ over different energies E_i, and can be corrected to yield true spectra $[I_{ti}(E_i)]$ simply by dividing by ε, or

$$I_{ti}(E_i) = [\varepsilon(I_{mi})]^{-1} I_{mi}(E_i) \equiv \delta(I_{mi}) I_{mi}(E_i), \tag{3}$$

where the quantity $\delta(I_{mi})$ is defined by this equation.

Some measured vs. true countrates derived in this way are shown in Figure 1(c), and at minimum a significant quadratic correction term is evident. This procedure has been used in a prior analysis of detector non-linearity by Kay and co-workers [7,8], and it is found to yield excellent correction for such effects in the Scienta system, including the MARPE data discussed previously.

2. Analysis of broad-scan survey spectra at different incident x-ray fluxes:

Consider a set of N survey spectra $I_{mi}^j(I_x^j, E_j)$ measured on the same sample, with incident fluxes $j = 1, 2, \ldots, N$, as illustrated shown in Figure 1(a). The intensities here span a range of approximately 40x, thus sampling the detector response very fully. We further assume that the true countrate I_{ti}^j (minus dark current as needed) for a given flux I_x^j, and energy E_i, can be expressed via a simple proportionality to flux, and that the true spectra can also be described by another power series in the measured spectra, as

$$I_{ti}^j(I_x^j, E_i) = I_x^j I_0(E_i) = \sum_{k=1}^{P} a_i I_{mi}^k(E_i), \tag{4}$$

where $I_0(E_i)$ = the true spectral shape in energy, $j = 1, 2, \ldots, N$; $i = 1, 2, \ldots, M$ = no. of channels in energy, and P is the maximum order of the polynomial needed to adequately describe the data (roughly 9 as a conservative number). Further assuming that the detector is linear at very low count rates such that, and then substituting for I_{ti}^1 and rearranging, permits expressing the data for all N spectra as:

$$\underbrace{-\left[\frac{I_{mi}(I_x^1, E_i)}{I_x^1} - \frac{I_{mi}(I_x^j, E_i)}{I_x^j}\right]}_{=\mathbf{B}} = \sum_{k=2}^{P} \underbrace{\left[\frac{I_{mi}^k(I_x^1, E_i)}{I_x^1} - \frac{I_{mi}^k(I_x^j, E_i)}{I_x^j}\right]}_{=\mathbf{M}} \underbrace{a_i}_{=\mathbf{A}}. \tag{5}$$

In matrix form, $\mathbf{B}$ is an $(N-1)\bullet M$ long column vector, $\mathbf{M}$ an $(N-1)\bullet M$ by $(P-1)$ matrix, and $\mathbf{A}$ a $(P-1)$ long column vector. Eq. (5) is an over-determined system of linear equations and can be solved for the maximum likelihood a_i's in $\mathbf{A}$ by finding the minimum of $|\mathbf{B} - \mathbf{MA}|^2$, *i.e.* by solving for $0 = \nabla_A|\mathbf{B}-\mathbf{MA}|^2 = 2\mathbf{M}^\mathbf{T}\mathbf{M} - 2\mathbf{M}^\mathbf{T}\mathbf{B}$ (superscript $\mathbf{T}$ = transpose). The polynomial coefficients in can by obtained by a standard "LU" decomposition [11] or simply by matrix inversion:

$$\mathbf{A} = (\mathbf{M}^\mathbf{T}\mathbf{M})^{-1}\mathbf{M}^\mathbf{T}\mathbf{B}. \tag{6}$$

where $\left(\mathbf{M}^{\mathrm{T}}\mathbf{M}\right)$ is a small $\left(P-1\right)$ by $\left(P-1\right)$ matrix. For better numerical precision in the matrix inversion, the measured counts should vary from 0 to 1, which can be achieved by trivial normalization.

Some results obtained with both methods are shown in Figure 1(d), where the true counts are plotted as a function of measured counts, and essentially identical results for the curve are found from both methods. Finally, in Figure 1(b), we show the same spectra as Figure 1(a), but with the correction applied: it is clear that all normalized spectra for different fluxes coincide to a high accuracy, thus permitting quantitative spectroscopy to be performed with this detector.

CONCLUSIONS

In summary, we have presented two distinct methods for correcting for non-linearity in detection systems, and demonstrated their validity for the specific case of the Scienta SES 200 spectrometer. Applications to this and other spectrometer systems for electrons and soft x-rays should be possible.

REFERENCES

1. (a) M.P. Seah, M. Tosa, Surf. Interface. Anal. **18** (1992) 240; (b) M.P. Seah, I.S. Gilmore, S.J. Spencer, J. Electron Spectrosc. **104** (1999) 73-89.
2. M.P. Seah, M.Tosa, Surf. Interface. Anal. 18 (1992) 240; (b) M.P. Seah, I.S. Gilmore, S.J. Spencer, J. Electron Spectrosc. 104 (1999) 73-89.
3. A. Kay, E. Arenholz, B.S. Mun, F.J. Garcia de Abajo, C.S. Fadley, R. Denecke, Z. Hussain, and M.A. Van Hove, *Science* **281**, 679(1998).
4. E. Arenholz, A.W. Kay, C.S. Fadley, M.M. Grush, T.A. Callcott, D.L. Ederer, C. Heske, and Z. Hussain, *Phys. Rev. B* **61**, 7183 (2000).
5. A. Kikas, E. Nommiste, R. Ruus, A. Saar, and I. Martinson, Sol. St. Commun. **115**, 275 (2000).
6. (a) M.G. Garnier, N. Witkowski, R. Denecke, D. Nordlund, A. Nilsson, M. Nagasono, and N. Mårtensson, and A. Föhlisch, Maxlab Annual Report for 1999 and private communication correcting this data; (b) D. Nordlund, M.G. Garnier, N. Witkowski, R. Denecke, A. Nilsson, M. Nagasono, N. Martensson, A. Fohlisch, Phys. Rev. B 63, 121402 (2001).
7. A.W. Kay, Ph.D. dissertation (University of California-Davis, September, 2000), Chapters 4 and 5.
8. A.W. Kay, F.J. Garcia de Abajo, S.H. Yang, E. Arenholz, B.S. Mun, M.A. Van Hove, Z. Hussain, and C.S. Fadley, Physical Review B **63**, 5119 (2001), and Proceedings of the Eighth International Conference on Electronic Spectroscopy and Structure, J. Electron Spectrosc. **114**, 1179 (2001).
9. N. Mannella et al., private communication.
10. D. Dessau and Y. Chuang, private communication.
11. W. H. Press, S. A. Teukolsky, W. T. Vetterling, B. P. Flannery, "Numerical Recipes in C: The Art of Scientific Computing", Cambridge University Press, New York, 1992, pp. 43-50.

This work was supported by the U.S. Department of Energy, Office of Science, Office of Basic Energy Sciences, Materials Sciences Division, under Contract No. DE-AC03-76SF00098..

Principal investigator: Norman Mannella, Department of Physics UC Davis, and Materials Sciences Division, Lawrence Berkeley National Laboratory. Email: norman@electron.lbl.gov. Telephone: 510-486-5446

Figure 1. (a) Survey spectra from a Cu(110) sample, obtained with AlKα excitation at various x-ray powers and constant voltage, normalized to be equal at the lowest countrates near zero binding energy. (b) Survey spectra for the four lowest power settings after non-linearity correction. (c) Plot of true countrate vs. measured countrate, as derived from Method 1. Countrates expressed in Hz per pixel in the CCD camera [7,8]. (d) Plot of measured countrate vs. true countrate as derived from both Methods 1 and 2.

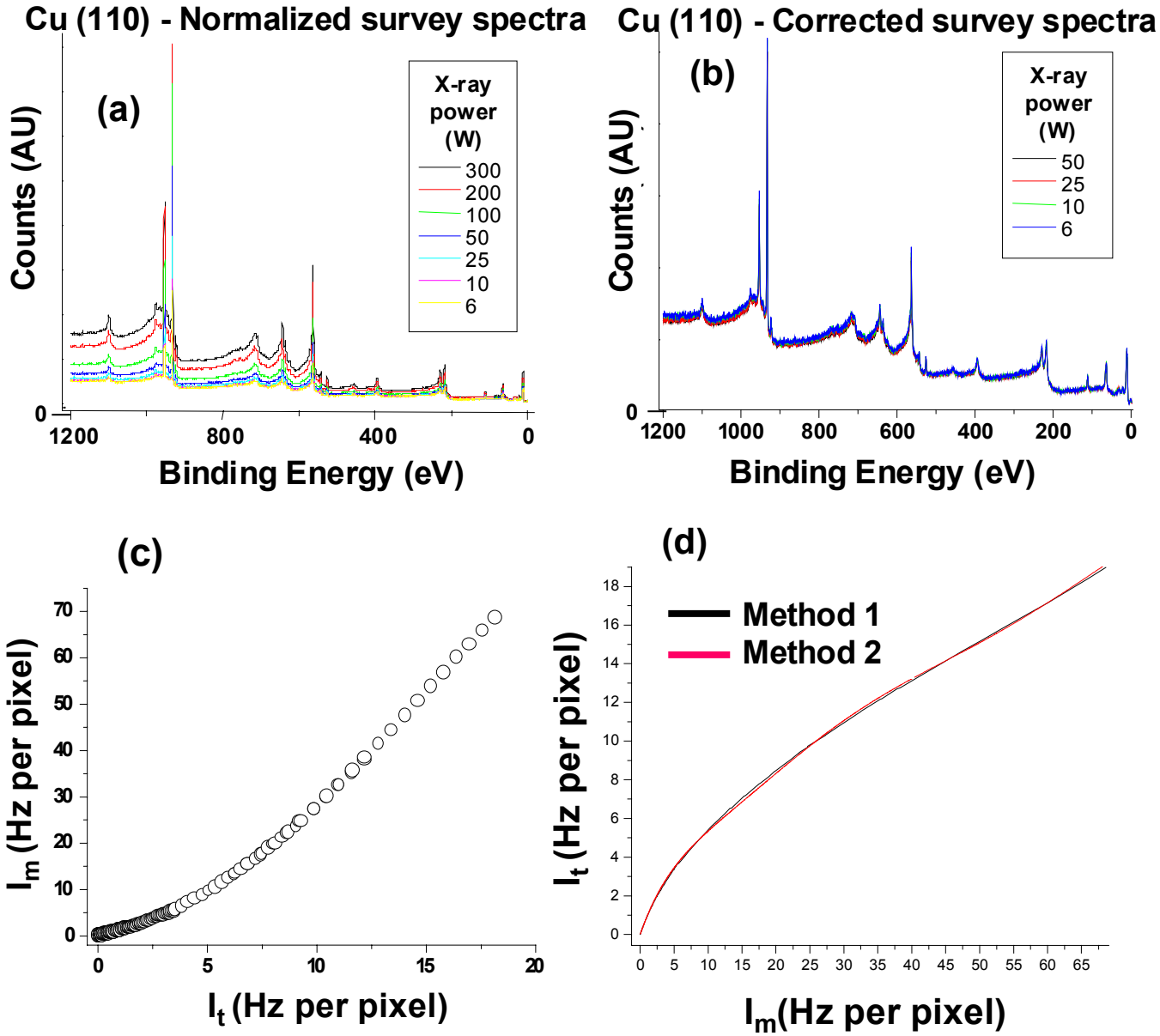

Development of a GHz-Rate Detector for Synchrotron Radiation Research

B. Turko[3], M. Press[3], A.W. Kay[1,2,#], M. West[1,3], J.E. Katz[3], H. Spieler[5], Z. Hussain[4], C.S. Fadley[1,2], B. Ludewigt[3], J.-M. Bussat[3], P. Denes[3], H. von der Lippe[3], G. Meddeler[3], G. Zizka[3], G, Lebedev [4], M. Mellon[6], T. Wiell[7]

[1]Materials Sciences Division, LBNL, Berkeley, CA 94720
[2]Dept. of Physics, UC Davis, Davis, CA 95616
[3]Engineering Sciences Division, LBNL
[4]Advanced Light Source, LBNL, Berkeley, CA 94720
[5]Physics Division, LBNL, Berkeley, CA 94720
[6]Quantar Technology, Santa Cruz, CA
[7]Gammadata/Scienta AB, Uppsala, Sweden
[#]Present address: Intel Corporation, Portland, OR

INTRODUCTION

It has by now become obvious that the brightness of third-generation synchrotron radiation sources often exceeds the capabilities of the end-station detector systems to adequately handle the electron or photon fluxes resulting from a given experiment, thus preventing both the fullest utilization of the radiation and the carrying out of certain new types of experiments readily, if at all. Detector non-linearity is one problem that has been encountered [1], but there are many other examples for which beamline or spectrometer throughput must be decreased to prevent high countrate saturation, or the number of energy or angular channels that can be counted simultaneously severely limits a given experiment [2]. In recognition of this, a national-level initiative in detector development has been proposed by the multi-institutional "DetectorSync" group [2].

As a first example of what can be accomplished with advanced detector technology, a project to develop an ultrahigh-speed one-dimensional detector for electrons and vuv/x-ray photons is underway at the ALS.

DESIGN PHILOSOPHY AND FIRST TEST RESULTS

This project takes advantage of unique expertise at LBNL for detector development in high-energy and nuclear physics, and involves the custom design and fabrication of application-specific integrated circuits (ASICs). The final goal is a 768-channel detector with 50 micron spacing between channels and a maximum linear countrate per channel of over 2 megaherz. The overall countrate will thus be in the 2 GHz range, and approximately 100 times faster than any other present one-dimensional or two-dimensional detector, with significantly improved spatial resolution as well compared to other existing detectors. First applications will be in electron spectroscopy, but others in x-ray absorption and x-ray emission spectroscopy are expected to follow.

A first prototype of this detector is shown in Fig. 1(a). Based on 12 pairs of 64-channel ASICs (an existing high-energy preamplifier chip (SDC) and a specially-designed buffered counter (DBC)), this detector has already demonstrated the ability to take spectra in a Scienta electron spectrometer located at the ALS (Fig. 2(a)), to resolve channels with a FWHM of 75 microns (Fig. 2(b)), and to count linearly at up to 1.0 GHz overall (Fig. 2(c)) [3].

Based on this experience, a next-generation detector with significant improvements in all elements from power supplies to ASICs to data acquisition is presently under development, with an expected completion date of late 2002. This will use 6 pairs of 128-channel ASICs (a newer high-energy preamplifier chip (CAFÉ-M) and a specially-designed buffer counter (BMC)), with optical coupling between detector and control/counting electronics to minimize noise and transients. The completion date for this project is estimated to be late 2002.

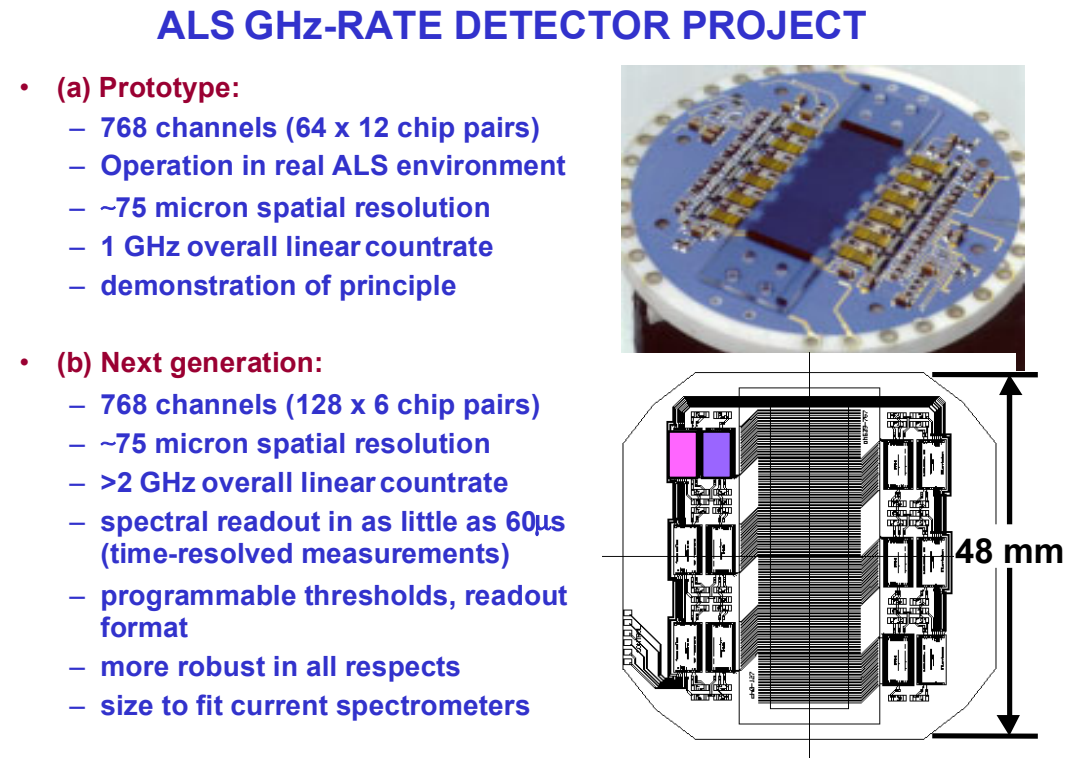

Figure 1--(a) Basic characteristics of the prototype GHz-rate detector developed as the first stage of this project, together with a photo of the ceramic substrate with 12 preamp-plus-counter chipsets mounted on it. The microchannel plates are not yet installed. (b) Basic characteristics of the next-generation detection now being designed and fabricated, together with a layout of its 6 chipsets and an indication of its size.

CONCLUSIONS

A prototype one-dimensional electron and photon detector operating linearly up to the GHz countrate level and with a resolution of 75 microns over 768 channels has been successfully developed and tested. An improved version of this detector is under development, with the same resolution and number of channels, but improved performance, programmability, and robustness in general user environments relative to the prototype. The next-generation detector should find use in several areas of synchrotron radiation research.

REFERENCES

[1] A.W. Kay, F.J. Garcia de Abajo, S.-H. Yang, E. Arenholz, B.S. Mun, N. Mannella, Z. Hussain, M.A. Van Hove, and C.S. Fadley, Phys. Rev. B 63, 115119 (2001); D. Nordlund, M.G. Garnier, N. Witkowski, R. Denecke, A. Nilsson, M. Nagasono, N. Martensson, A. Fohlisch, Phys. Rev. B 63, 121402 (2001); and abstract in the 2001 Compendium by N. Mannella et al.

[2] Local participants in the DetectorSync initiative include A. Thompson, H.A. Padmore, and C.S. Fadley, and the group's website is at--http://www-esg.lbl.gov/esg/meetings/detectorsync/index.html, with a more detailed white paper on detector needs also downloadable from this source.
[3] A.W. Kay, Ph.D. thesis (University of California, Davis, September, 2000), LBNL report 46885, and to be published.

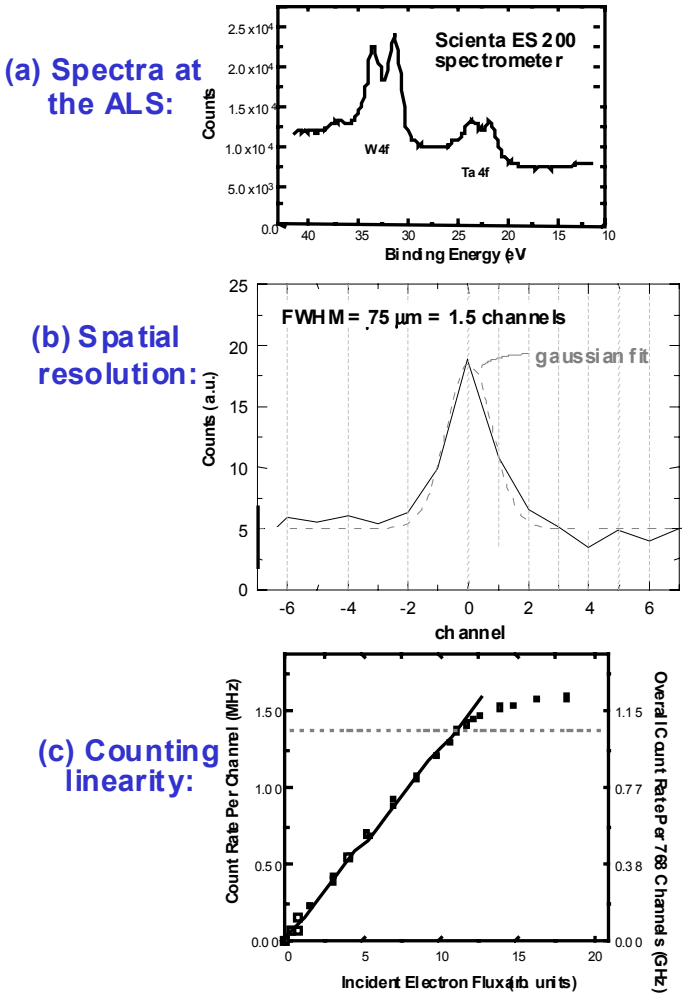

Figure 2--Test data from the first prototype detector shown in Fig. 1(a). (a) Test spectra obtained with the detector mounted in a Scienta SES 200 spectrometer at ALS beamline 9.3.2. (b) Spatial resolution determination via a collimated electron beam source. Each channel is 50 microns. (c) Counting linearity per channel (ledt scale) and over all channels (right scale) as determined with an electron gun.

This work was supported by the U.S. Department of Energy, Office of Science, Office of Basic Energy Sciences, Materials Sciences Division, under Contract No. DE-AC03-76SF00098..

Principal investigator: Charles S. Fadley, Department of Physics UC Davis, and Materials Sciences Division, Lawrence Berkeley National Laboratory. Email: fadley@lbl.gov. Telephone: 510-486-5774

High Resolution XPS investigation of Oxide layer grown on Ge substrates

N. Tabet [(a)] , M. Faiz [(a)] , N.M. Hamdan [(b)] and Z. Hussain [(b)]

[(a)]Surface Science Laboratory, Physics Department, King Fahd University of Petroleum and Metals, Saudi Arabia.
[(b)]Lawrence Berkeley National Laboratory, Advanced Light Source, Berkeley, CA 94720

Abstract

We present an XPS study of thin oxide layers grown by thermal oxidation of germanium substrate at T = 380 ºC, under 400 mTorr of dry air. The samples were mechanically then chemically polished prior to the heat treatments. Ge3d, O1s and C1s lines were recorded after successive cycles of ion etching at low Argon pressure. The Ge3d spectra showed a shift of the oxidized germanium peak from 33.2 eV to 31.5eV binding energy while the peak corresponding to the non-oxidized germanium atoms of the substrate remains fixed at 29.2eV. The analysis of a GeO_2 amorphous sample showed no shift in the binding energy of the Ge peaks. The 31.5 eV binding energy peak observed during the analysis of the oxide layer grown on germanium substrate was attributed to the formation of a stable GeO phase under argon bombardment. In addition, the results showed the emergence of a carbon peak of low binding energy (E_b=282.3eV) at the interface Ge/GeO_2. This peak was attributed to the formation of carbides during the heat treatment.

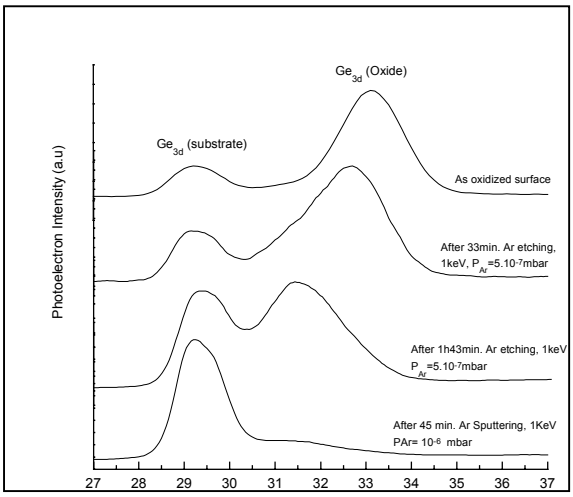

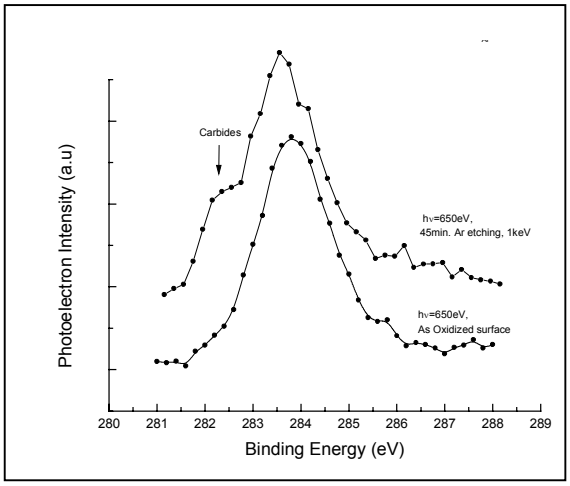

This work was supported by the Director, Office of Science, Office of Basic Energy Sciences, of the U.S. Department of Energy under Contract No. DE-AC03-76SF00098.

Contact person: Nasser Hamdan, E.O. Lawrence Berkeley National Laboratory.
Telephone: 510-486-7633. Email: nmhamdan@lbl.gov.

Optimization of PEEM-2 for studies of organic thin films

C. Morin[1], A.P. Hitchcock[1], H. Ikeura-Sekiguchi[1,2], A. Scholl[3], A. Doran,[3] K. Kaznacheyev[4]
[1]BIMR, McMaster University, Hamilton, ON, Canada L8S 4M1
[2]Quantum Radiation Division, Advanced Industrial Science and Technology (AIST), Tsukuba, 305-8568 JAPAN
[3]Advanced Light Source, Berkeley Lab, Berkeley, CA 94720
[4]Physics, CLS, University of Saskatchewan, Saskatoon, SK Canada S7N 5C6

INTRODUCTION

There are many potential applications of X-ray photoelectron emission microscopy (X-PEEM) to organic thin films, such as fundamental studies of phase separation [1], and applied studies of organic light emitting diodes, adhesion promoters [2] etc. In order to obtain meaningful results, it is important to understand the challenges of applying X-PEEM to organics, and to develop compensating data acquisition strategies. These challenges include: radiation damage, camera artifacts, Io determination, higher order radiation, charging, sample damage from field emission or discharges.

The photon flux at BL 7.3.1 ($>10^{12}$ photons/s at 500 eV in a 30x300 μm spot, with 1.9 GeV, 400 mA) is very high because there are only two optical elements and energy resolution is sacrificed for flux. The high flux, combined with a relatively inefficient electrostatic column (~5 % transmission at high spatial resolution – 12 μm aperture) and an inefficient camera, mean that ratio of detected signal to number of photons absorbed in the near surface region is very small. In order to perform useful chemical analysis, images of the region of interest must be recorded at a number of energies (in the C1s, N1s or O1s regions for organic samples) to form an image sequence which can be subsequently analysed to obtain point or region spectra, or chemical maps. Other problems occur because of limitations of the CCD camera - bad pixels; pixel-to-pixel variation in dark signal (leakage) and gain; as well as a slow data transfer rate (0.25s/image, no ability to transfer sub images). A further challenge is the uneven illumination in the PEEM; in order to gain sensitivity we use reduced magnification. Typically the camera views 60x60 μm^2 but only the central third of the image is illuminated.

In order to reduce the damage rate we work at much reduced flux, achieved by placing an aperture (formed by two independently adjustable elements, called 'chopper' and 'mask') in the beam before the monochromator. This reduces the energy resolution as well as the flux – at a chopper value of 15 the resolving power is only 100. Under typical low dose conditions we work with less than 10% of the dynamic range of the camera. Background and camera corrections are extremely challenging. It is essential to record Io spectra from a suitable reference surface, typically HF-etched silicon for organic thin film samples deposited on Si or Si_3N_4. This is especially true in the C 1s region where there is a lot of structure in the Io spectrum. The Io signal must be measured under very similar conditions to those used to study the sample in order to ensure the same sensitivity, energy resolution and higher order content, (the latter two depend on the exact choice of chopper, windows, slits and filters used). The PEEM sensitivity is very dependent on the sample-objective lens distance, which changes every time a sample is re-positioned.

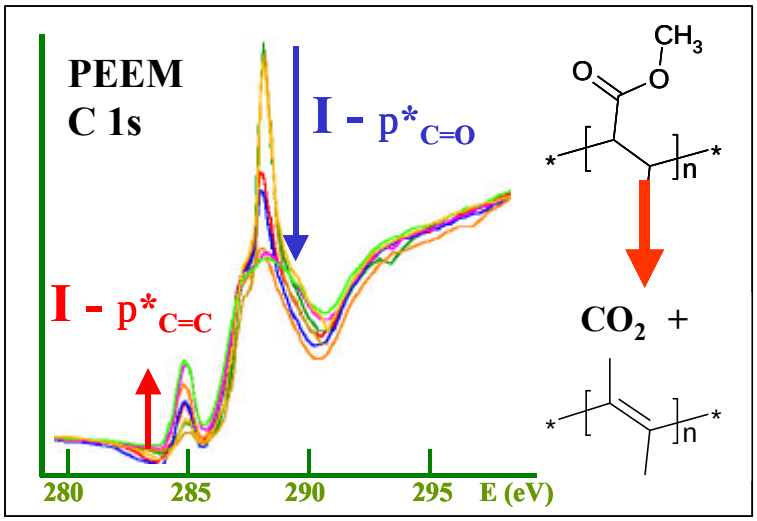

Fig. 1 Plots of C 1s NEXAFS of a 50 nm PMMA film on c-Si. Successive scans made on the same spot build up dose and damage.

Charging can occur for any insulating sample, although it is often surprising the samples that can be studied by PEEM. We typically observe charging if a polymer sample is too thick (> 75 nm), or too corrugated (> 15 nm rms). In some cases a thin metal coating (<2-3 nm) can be evaporated to control charging. Charging results in dark spots on images, where the electrons are trapped by the surface charge potential, or in bright spots, where there is artificially enhanced emission by discharges or, at locations of high curvature, by enhanced detection

probability due to stronger fields. While it is sometimes possible to record meaningful NEXAFS spectra from charging surfaces, more typically, charging results in large and variable sample or objective lens currents which lead to unstable operation, and, in extreme cases, macroscopic discharges that can damage samples, making dramatic dendritic patterns in organic layers, and exploding Si_3N_4 windows. In the following we describe a systematic study of a pure polymethylmethacrylate (PMMA) film in order to characterize its radiation damage rate, and thereby develop procedures to study heterogeneous samples containing PMMA in a meaningful fashion, despite these challenges. A detailed manual for operating X-PEEM and choosing parameters optimal for radiation sensitive samples is available at the beam line or from the authors [3].

EXPERIMENTAL

~50 µl of a 1.0% w/w toluene solution of PMMA (Mw = 112.3 K, Mw/Mn = 1.09, Polymer Source Inc) was passed through a teflon filter to remove particulate impurities and dropped onto a spinning HF-etched Si chip at 4000 rpm. Spinning was continued for ~5 s. The film thickness was estimated to be ~40 nm from AFM at a scratch and the rms roughness was 6 nm The sample was not annealed.

Property	Value	Property	Value
Mask	0.9	Dwell (s)	3
Chopper	15 or 16	Camera gain	normal, x8
Al window #1	in	PEEM aperture (µm)	50
Al window #2	in	Sample (kV)	18.0
Exit slit	in	Objective (kV)	13.68
Ti filter (150 nm)	in	Transfer (kV)	12.45
Flash light	on	Intermediate	13.78
Background (Hz)	50	Projection	0

The relationship of measured intensity to the various parameters controlling the signal is summarized in **equation 1**. A number of scale factors need to be determined but this qualitative formula may be useful for others using PEEM-2 for organic thin film studies.

$$S = G*t*[I*\sigma*f_{esc}*F*\varepsilon_{PEEM} - B] \quad \text{(eqn 1a)}$$

where S = detected signal , G = camera gain (2,4,8), t = time, σ = cross-section, f_{esc} = electron escape probability (integrated over inelastic scattering and angular effects), F = work function, ε_{PEEM} = PEEM column efficiency [α (magnification)* (aperture)^2], B = no-X-ray background, and I is the flux (ph/s) on the sample, given by

$$I \alpha\ I_{ring}*C*T \quad \text{(eqn 1b)}$$

where C, the chopper factor is $(C_{max}-C)/C_{max}$; and T, the Ti filter factor, is $(T_{max}-T)/T_{max}$.

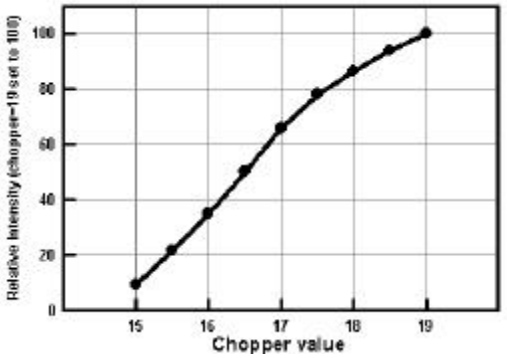

Fig. 2 Variation of flux on sample vs. chopper.

RESULTS AND DISCUSSION

Fig. 1 shows a typical sequence of spectra (without Io correction) recorded while the sample was being damaged. The relative radiation damage rate for PMMA in the low dose regime was determined by recording successive image sequences on the same spot, using the instrumental parameters listed in table 1. Only 24 energies in 283-295 eV range were used in order to track damage changes adequately. In general keeping the number of sampled energies to the minimum is a key step in making meaningful measurements of organics. The *relative dose* was obtained from the integrated spectral signal up to a given measurement, taking into account the dead time between images (~2 s). The *relative damage* was obtained from the increase in the area of the 285 eV $\pi^*_{C=C}$ peak (growth of reduced sites in the backbone) and decrease in the area of the 288 eV $\pi^*_{C=O}$ peak (loss of acrylate groups). In addition to the measurements made at low dose, another series at much higher dose (5 or 10 s exposure at chopper 19) was performed. The two sets were matched in the overlapping region of the 285 eV and 288 eV damage curves. Finally the dose scale was expressed in terms of time equivalent at full flux in the carbon 1s region using the variation of signal strength with chopper setting to scale the times (**Fig. 2**).

Fig. 3 plots damage versus relative dose for PMMA as measured in the PEEM As is typical in radiation damage curves, there is an exponential change with saturation. Based on these results, we estimate that, at the full flux dose rate (chopper = 19, 400 mA in the ALS), the total acceptable exposure time for meaningful measurements of samples containing PMMA with negligible damage (as measured by spectral change) is 10 seconds. Since it takes about 5 seconds to record an image of acceptable quality, if full flux is used it is only possible to record a few images before the PMMA in a PMMA-containing sample is irreversibly modified. We note that a recent study of radiation damage in various polymers by STXM [4] indicates that PMMA is about average in terms of radiation sensitivity.

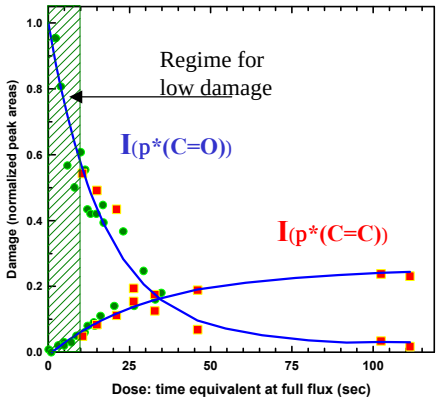

Fig. 3 Intensity at 288 eV and 285 eV versus accumulated radiation dose. The dose is time to equivalent deposited energy when PEEM is operated with full flux. The green points are measurements made at reduced flux. Chopper: green (15), red (19).

Chemical imaging with PEEM requires images at a number of energies.Typically 10-15 images are needed. The only way to get these without "frying the sample" is to "turn down the torch". We routinely do this by using the chopper to reduce the flux ~10-fold (see Fig. 2). This allows 10-20 images to be recorded prior to significant damage. Chopper values below 15 are not useable since the grating is inadequately illuminated. 2-bunch mode is also useful, but normalizing the rapid time variation of flux is a challenge.

Fig. 4 presents results of a low dose study of a 20:80 (w/w) PS:PMMA film (PS = polystyrene) which has domain sizes on the order of 250 nm as determined by prior AFM measurements. This is a continuation of our earlier studies of phase segregation on PS:PMMA blends [1]. We are trying to develop a metastable system with flat, reasonably large domains that are pure PS and PMMA, in order to carry out competitive protein adsorption studies. As the analysis of the spectrum of the PMMA-rich regions shows, the as-made material still contains significant PS, as found earlier [1]. However, with our refined understanding of the damage rate of PMMA in PEEM-2, we are now very confident that the 285 eV signal observed in the PMMA-rich domains is from incompletely phase segregated PS and NOT from the C=C bonds formed from radiation damage of PMMA (Fig 1).

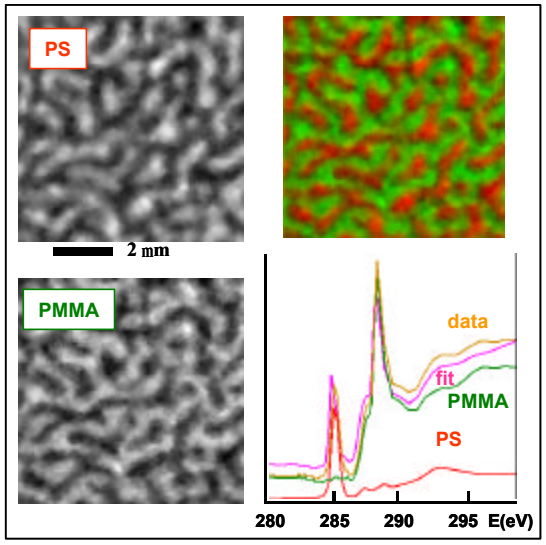

Fig. 4 PS and PMMA component maps, and color composite derived from image sequence of as-made 20:80 PS:PMMA blend, using low dose protocol (3s dwell, chopper=16, few points). Lower right shows the results of a curve fit to the spectrum of pixels in strong PMMA regions. (Jun-01).

SUMMARY: Relative dose - damage relationships for PMMA were measured in PEEM-2 to define an acceptable regime [5]. Similar calibration measurements are required prior to study of other radiation sensitive samples. Self-assembled monolayer and micro-contact printed systems involving fluorocarbons are particularly challenging due to their very small thickness (< 5nm) and extreme radiation sensitivity. An even more rigorous application of the methods outlined in this report is required for successful studies of such materials.

1. C. Morin et al, *J. Electron Spectrosc* 121 (2001) 203-224
2. G. E. Mitchell, et al. 1999 ALS Compendium (2000)
3. C. Morin, A.P. Hitchcock, H. Ikeura-Sekiguchi, A. Doran and A. Scholl, PEEM-2 manual (2001).
4. T. Coffey, S.G. Urquhart and H. Ade, *J. Electron Spectroscopy* 122 (2002) 65.
5. C. Morin, A.P. Hitchcock, et al in preparation.

Supported by NSERC (Canada) and Canada Research Chair program. ALS is supported by U.S. DoE (DE-FG02-89ER60858). Data analysis done with **aXis2000**, an IDL widget available at http://unicorn.mcmaster.ca/aXis2000.html

Principal investigator: *Adam Hitchcock*, McMaster, **aph@mcmaster.ca**. Ph: 905 525-9140

Soft X-ray emission spectroscopy of the liquid-solid interface between water and a $Cu(In,Ga)(S,Se)_2$ thin film solar cell absorber

C. Heske[1], U. Groh[1], O. Fuchs[1], L. Weinhardt[1], E. Umbach[1], Ch.-H. Fischer[2], Th. Schedel-Niedrig[2], M.Ch. Lux-Steiner[2], S. Zweigart[3], F. Karg[3], J.D. Denlinger[4], B. Rude[4], C. Andrus[5], and F. Powell[5]

[1]Experimentelle Physik II, Universität Würzburg, Am Hubland, D-97074 Würzburg, Germany
[2]Hahn-Meitner-Institut, Glienicker Str. 100, D-14109 Berlin, Germany
[3]Siemens & Shell Solar GmbH, SSSG T, Otto-Hahn-Ring 6, D-81739 München, Germany
[4]Advanced Light Source, 1 Cyclotron Rd., Berkeley, CA 94720
[5]Luxel Corp., 515 Tucker Ave., Friday Harbor, WA 98250

INTRODUCTION

The development of experimental methods to probe the properties of liquid-solid interfaces is one of the fundamental issues for understanding a multitude of natural and technological processes involving liquids. Up to date, however, very few experiments have been performed to learn about the electronic structure, particularly if an atom-specific point of view is desired. While in surface science such information can easily be derived from photoelectron spectroscopy, this approach is not viable for the study of liquid-solid interfaces due to the limited information depth of PES. Thus, the necessity to probe "through" a liquid (or solid) layer calls for photon-in-photon-out experiments. The soft X-ray regime, however, which is the most suitable to study core and valence states of light elements, has not yet been explored, mostly due to the high attenuation of soft X-rays in matter. In this report we demonstrate that soft X-ray emission spectroscopy (XES) can be used to investigate the chemical and electronic properties of particular atoms at liquid-solid interfaces, in this case the water–$Cu(In,Ga)(S,Se)_2$ interface. Furthermore, we will show that, with XES, it is possible to monitor interfacial chemical reactions with high spectral resolution *in-situ*.

MATERIAL SYSTEM

$Cu(In,Ga)(S,Se)_2$ (CISSe) is widely used as an absorber material in thin film solar cells, and conversion efficiencies up to 18.8 % have been achieved [1]. Apart from being a model system for the present investigation, the water–CISSe interface is of large importance for two reasons. First, a complete CISSe solar cell is comprised of several thin film layers, including the CISSe absorber layer and a thin (approx. 20 nm) CdS buffer deposited in a chemical *bath* deposition process. The CdS/CISSe interface plays one of the central roles in understanding the electronic structure of the devices. Hence, the possibility to study liquid-solid interfaces *in-situ* allows the monitoring of the substrate, the growing film, and the interface formation process from a spectroscopic point of view. Secondly, one of the main issues on the way to a complete industrial product is the control of humidity impact on the electronic cell properties. The investigation of the relevant water–solid interfaces is expected to shed light on the chemical and electronic changes induced by the humidity on an accelerated time scale.

EXPERIMENTAL

High-resolution soft X-ray emission spectroscopy was performed at beamline 8.0 utilizing the SXF endstation. Beamline 8.0 allows experiments with an excitation photon flux of about 4 x

10^{15} photons/sec near the sulfur $L_{2,3}$ edge. Thin films of CISSe were prepared in a rapid thermal process of elemental precursor layers on Mo-coated soda-lime glass in a sulfur-containing environment. The experiments were performed in ultra-high vacuum (UHV) utilizing suitably designed stainless steel liquid cells, which were glued to the CISSe sample surface with a UHV-compatible epoxy. In the design of the liquid cells, a channel of 1.3 μm of liquid water was created between the CISSe surface and a 1 μm-thick polyimide (PI) window. After hardening of the epoxy (approx. 24 hours), the complete assembly was transferred into UHV for experiments. Reference experiments were also conducted on "bare" CISSe films as well as on PI/Vacuum/CISSe sandwich structures.

RESULTS

Fig. 1 presents a set of sulfur $L_{2,3}$ emission spectra obtained by excitation well above the absorption edge ($h\nu$ = 200 eV). The bottom spectrum was obtained from the "bare" CISSe film surface, i.e., taken directly from the solar cell production line. Peak (1) stems from the emission of sulfur atoms bound in a sulfide environment, and is due to photons emitted by filling S 2p core holes with S 3s electrons [2]. Peaks (2) are associated with the same electronic transition, but for sulfur atoms bound to oxygen. In the present case, the absence of an additional peak around 161.1 eV indicates that at most two oxygen atoms are bound to each probed sulfur atom. The broad peak (3) is due to Cu 3d states in the upper valence band of CISSe and, because of the local nature of the excitation, is indicative of sulfur-copper bonds. In short, the spectral features of the sulfur XES spectrum give a wealth of detailed information about the local chemical bond of the sulfur atoms, which can now be used to monitor interfacial processes.

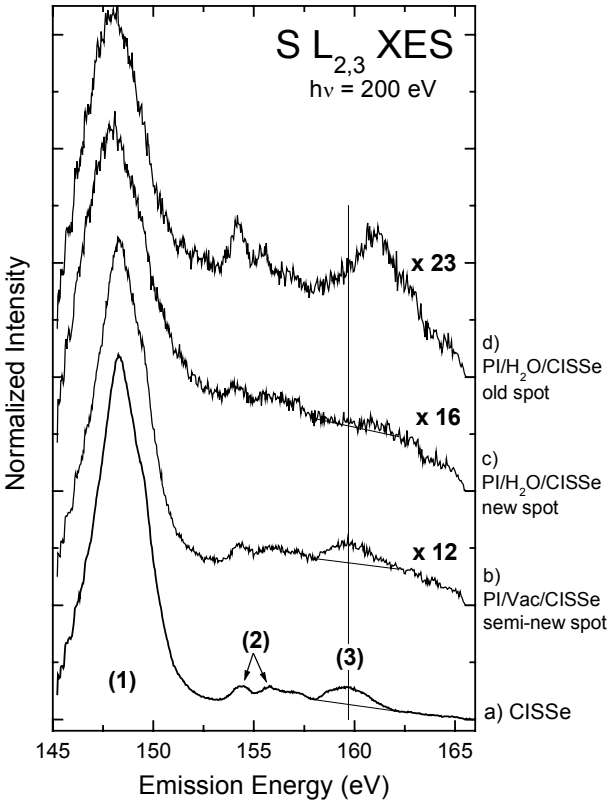

Figure 1. S $L_{2,3}$ X-ray emission spectra of a $Cu(In,Ga)(S,Se)_2$ (CISSe) thin film solar cell absorber film (a) taken from the production process, (b) seen through a 1 μm polyimide (PI) window, and under an additional 1.3 μm water layer (c: new sample spot, d: old sample spot). Samples "under water" show a reduced intensity of the S-Cu-bond and, after X-ray exposure, a sulfate formation.

As indicated in Fig. 1 by the magnification factors at the right hand side, the observed signal intensity is reduced by both the PI window as well as the liquid water layer. These attenuation factors indicate the necessity to use high-flux excitation from a third generation synchrotron source. Note that the PI window is damaged by extended exposure to X-rays. Thus, the transmission decreases as a function of exposure within the probed area, and hence the "age" of the spot also factors into the signal attenuation. The "age" of the different spectra is given on the right-hand side of Fig. 1. A closer inspection of spectra a) and b) reveals that no changes are observed for the PI/Vacuum/CISSe sample (as expected). However, we find a reduction of the intensity associated with sulfur-copper

bonds (peak 3) due to the 24 hour storage "under water" (spectrum c). An even more pronounced spectral change is observed after exposure to X-rays (30 min, spectrum d). Based on the strong S 3d-related emission at 161.1 eV, this spectral change is interpreted as a sulfate formation at the water/CISSe interface.

Apart from a detailed look at the chemical and electronic environment of sulfur atoms, also the Na K_α emission line proves to be a helpful tool to monitor the interfacial reaction at the water/CISSe interface. Na-assisted growth has been shown to substantially improve the efficiency of the CISSe solar cells. Until today, the impact of the Na has not been fully clarified, mostly because several enhancing mechanisms have been proposed and because, due to the complexity of the system, these different mechanisms are not easily separable. An established model by Kronik et al. [3] suggests an interaction of sodium and oxygen at the CISe surface. Nevertheless, apart from a co-adsorption study in ultra-high vacuum [4], no direct experimental evidence of a chemical interaction between sodium and oxygen has yet been reported. Such a direct correlation can now be derived from a simultaneous recording of Cu L_α and Na K_α XES spectra. As expected, we find a small Na signal on the CISSe surface, which does not change in intensity for the PI/Vacuum/CISSe sample. Also, the 24-hour storage under water only leads to a small increase. In contrast, when exposing the sample to the soft X-ray beam, we find a dramatic increase of the Na content at the interface in the course of time, in parallel with the above-discussed surface oxidation (sulfate formation). Apparently, the possibility to form a sulfate species attracts Na atoms from the CISSe film towards the surface. Here, the original driving force could be the X-ray-induced creation of O^{2-} and/or OH^- ions, which then react with the CISSe surface and alter the free energy, such that Na atoms diffuse to the water/CISSe interface. Also the opposite process, namely that the X-ray excitation attracts Na atoms to the surface (e.g., by sample heating), which then act as a catalyst for the surface oxidation, appears possible. Future studies utilizing mini-cells with integrated thermocouples will have to clarify which one of the two scenarios holds true.

In summary, we have presented an experimental investigation of a sulfate formation at the water/CISSe interface. The findings demonstrate that there is a direct correlation between oxidation and sodium enrichment at the interface. The demonstrated general approach of utilizing X-ray emission spectroscopy to study chemical reactions in-situ can be extended to many other liquid-solid interfaces and also lends itself to the study of liquids and solutions as well.

REFERENCES

1. M. A. Green, K. Emery, D. L. King, S. Igari, and W. Warta, Solar Cell Efficiency Tables (Version 17); Progr. Photovolt. Res. Appl. **9**, 49 (2001).
2. C. Heske, U. Groh, O. Fuchs, E. Umbach, N. Franco, C. Bostedt, L.J. Terminello, R.C.C. Perera, K.H. Hallmeier, A. Preobrajenski, R. Szargan, S. Zweigart, W. Riedl, and F. Karg, phys.stat.sol. (a) **187**, 13 (2001).
3. L. Kronik, D. Cahen, and H.W. Schock, Adv. Materials **10**, 31 (1998).
4. C. Heske, G. Richter, Zhonghui Chen, R. Fink, E. Umbach, W. Riedl, and F. Karg, J. Appl. Phys. **82**, 2411 (1997).

This work was supported by the german ministries BMBF (FKZ 01SF007) and BMWI (FKZ 0329889, FKZ 0329218C), as well as the DFG through SFB 410, TP B3.

Principal investigator: Clemens Heske, Eberhard Umbach, Experimentelle Physik II, University of Würzburg, Germany. Email: heske@physik.uni-wuerzburg.de. Telephone: ++49-931-888-5127.

Use of Synchrotron Reflectance Infrared Spectromicroscopy as a Rapid, Direct, Non-Destructive Method for the Study of Inks on Paper

T. J. Wilkinson[1], D. L. Perry[1], M. C. Martin[1], W. R. McKinney[1], and A. A. Cantu[2],
[1]Lawrence Berkeley National Laboratory, Berkeley, CA 94720
[2]U. S. Secret Service, U. S. Department of the Treasury, Washington, DC 20373

INTRODUCTION

The analysis of inks and the paper to which they are applied is of great interest to a broad spectrum of science. From the historian and archaeologist to the forensic scientist, an understanding of ink-paper interactions is essential to the understanding of the ink and its subsequent changes upon application to paper. Determining chemical and other details of ink in a signature, for example, can be an exceedingly difficult task. Modern ballpoint writing inks are frequently mixtures of ink vehicles (used to dissolve the dyes or disperse pigments), dyes and/or pigments, various resins and polymers (to control the viscosity of the ink and to serve as "fillers"), acidic materials (frequently fatty acids that function as lubricants), and surface-active agents. Additionally, other organics may be used to control corrosion or improve solubility of the dyes and pigments.

From the moment that a writing ink is applied to paper material, both the chemical composition of the ink and the ink/paper interface begin to undergo changes. Various physical and chemical processes occur, including the evaporation of solvents and other volatile compounds, polymerization, oxidation, cross-linking, and, in some cases, paper corrosion. These processes can also include those that are effected by external factors such as heat and light, with possible chemical reactions being photolytically induced. Other interactions with the paper are possible.

In the present work, the use of synchrotron radiation-based infrared (SR-FTIR) spectromicroscopy offers a powerful, non-destructive method for the study and identification of inks on paper and the comparison of them to one another without the need for chemical separations and related laboratory work. Also, this method allows for a detailed analysis without the inherent destruction of the ink samples on the paper by more commonly used technique**.**

EXPERIMENTAL

The ink/paper combinations were analyzed using infrared Beamline 1.4.3 at the Advanced Light Source (ALS) at Lawrence Berkeley National Laboratory. All spectra were obtained using collimated synchrotron light directed into a Nicolet Magna 760 FT-IR bench. The deconvolution work of several of the parent ink infrared spectra was performed using the Nicolet software in conjunction with search libraries from Sigma-Aldrich that are copyright-assigned to Nicolet. All samples were analyzed by collecting a minimum of 256 scans in the mid-IR range (4000-400 cm^{-1}). Residual water and carbon dioxide were subtracted where appropriate, and baselines were normalized using the correction routines present in the software.

To prepare samples for infrared study, ink was applied to paper strips (~2.5 cm x 5 cm). The paper strips were placed on the infrared microscope sample holder and were measured in reflectance mode. The paper used was measured to have a transmittance of < 1% throughout the mid-IR, so reflection-absorption (IR passing through the paper, reflecting off the microscope stage, and then passing back through the paper) can be ruled out. The measurements obtained were therefore dominated by specular reflectance, with some diffuse reflected light collected as well. Also, some ink component compounds were identified by taking the spectra of the ink that had been directly applied to a silver coated microscope slide [Kevley Technologies, Chesterland, OH

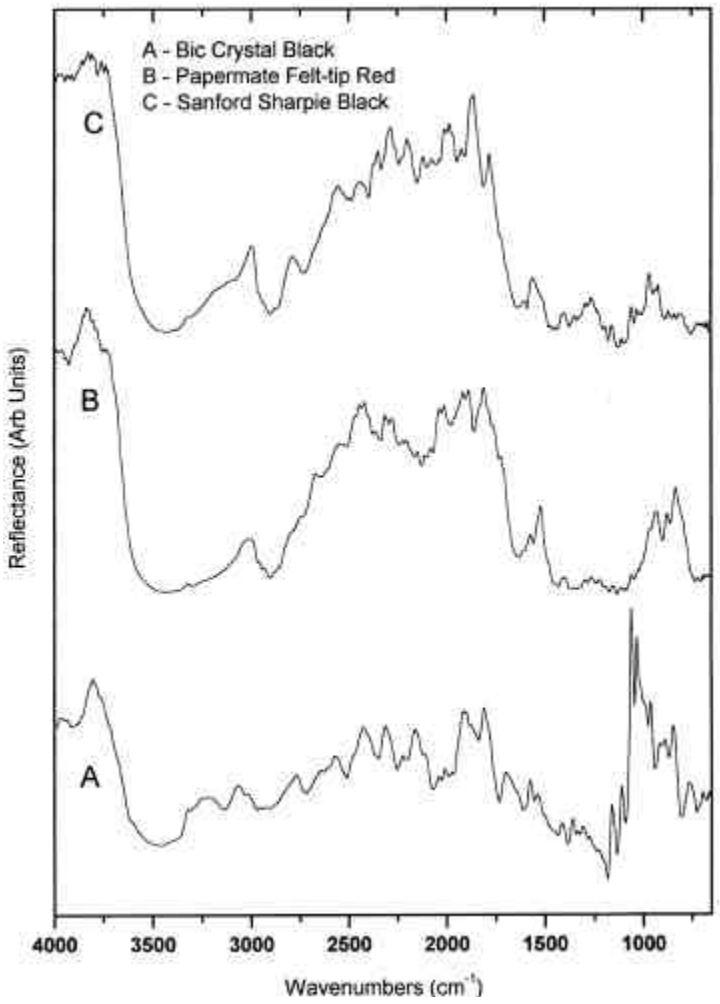

Figure 1. Infrared spectra of a) a commercial black ink, b) a commercial red ink, and c) another commercial black ink all on the same Whatman 3MM Chr chromatography paper.

RESULTS AND DISCUSSION

As mentioned above, the chemistry of inks in commercial pens is highly complex, and as a result, the infrared spectra of the inks tend to be quite complicated because of the overlap of many of the vibrational bands from the different constituents. Figure 1 shows the infrared spectra of three typical commercial inks on a high-purity chromatographic paper. All of the spectra exhibit bands which are common to many compounds that are typically used in ink formulations. One readily assignable area of the spectrum is the 2900-3000 cm^{-1} region associated with the υ(C-H) stretch for aliphatic hydrocarbons. The ~ 3500 cm^{-1} region is associated with the υ(OH) stretch of water and alcohol solvents that are typical for many ink systems. More complicated, however, is the ~ 800-1700 cm^{-1} "fingerprint region" in which many of the ink constituents' infrared spectra overlap with one another. In yet another region (1700-3500 cm^{-1}) for blue, black, and red inks such as shown in Figure 1, the spectra are seen to be equally complex. All of these regions contain multiple vibrational bands such as C=C, C=N, C-O, C=O, C-N, C-S, S-O, ring modes (both aromatic and aliphatic), and combination bands from the dozens of compounds that constitute each ink.

The use of synchrotron-based FT-infrared microspectroscopy described herein for the study of inks and their interactions with paper affords several advantages over other experimental and spectroscopic approaches. First, it is a direct method with no necessity for any pre-chemical separations such as chromatography. Second, the technique represents a method for obtaining a molecular fingerprint of different inks that make them easily and readily distinguishable. Third, it offers an extremely high lateral spatial resolution of less than 10 μm, much smaller than any line made on paper by normal ball point or fountain pens and much smaller than the "worst case" situation for examining ink samples on paper ("...probably the true worst case is the examination of a single dot..."). Fourth, the sensitivity of the synchrotron-based infrared technique is 200 times greater than a regular FT-infrared instrument for a 10 μm spot size, thus making it possible to see spectroscopic detail in some instances that would be missed by traditional spectrometers. Fifth, because of the mapping capability relative to the spatial resolution of the synchrotron spectromicroscopic technique, it is possible to study infrared spectroscopic profiles of the actual line interfaces of the different inks in a line or signature on paper (actually, spectroscopically seeing where one ink ends and another begins in the same signature, for example).

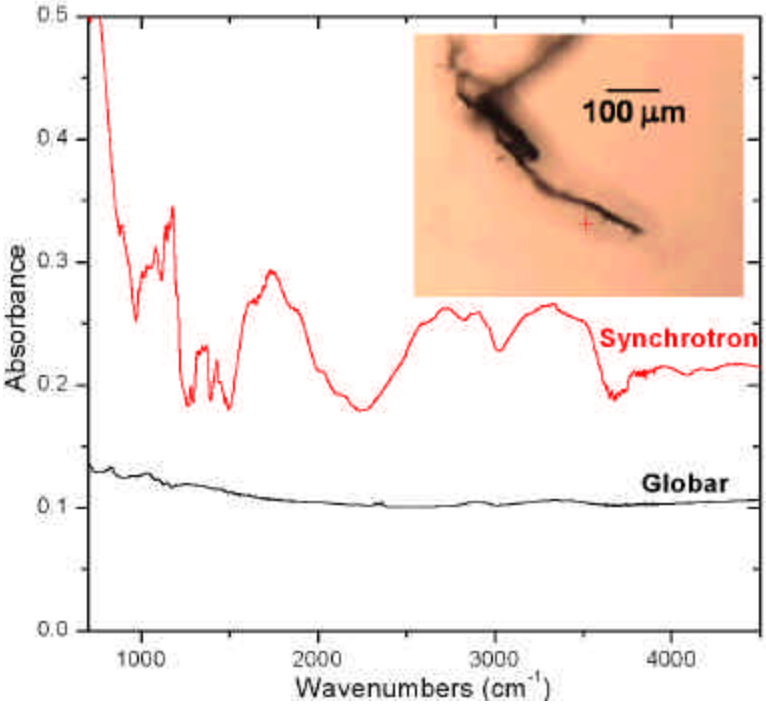

Figure 2. Infrared spectra of ink on a paper fiber using both synchrotron and Globar™ infrared sources. The difference in the two spectra is due to the much greater brightness of the synchrotron impinging on the fiber.

The issue of sensitivity and resolution as advantages to using synchrotron-based FTIR spectro-microscopy over traditional stand-alone infrared instrumentation for the study of ink on paper is dramatically illustrated in Figure 2. The inset photograph shows ink on a paper fiber being studied using both a synchrotron infrared source on Beamline 1.4.3 at the ALS and a Globar™ infrared source. The two spectra shown were taken using the two different infrared sources represent an ink spot on the paper fiber of ~10 microns, and they were taken using the same number of scans. The superior sensitivity and resolution of the synchrotron-based approach shown in Figure 2 emphasizes the nearly unlimited possibilities for the use of the techniques for looking at very small, fragmentary samples of ink on paper and for other ink/paper systems such as printed material.

Two comments should be made on the use of background subtraction. First, paper, even the same brand and type, is never pure or totally reproducible at the micron level. Paper batches are processed from different pulp sources blended together for the final product. Thus, there is a very high probability that a point analysis on the same sheet of paper may differ slightly. Second, when one microscopically examines ink on paper from a pen applied under normal writing conditions, one sees both paper and ink, not just an area of paper covered totally by the ink. The ratio of the ink-to-paper area being studied in a several micron area may vary. In any rigorous study of ink/paper combinations, an investigator should take a sampling of locations on the ink/paper line so as to get a more complete and truer spectromicroscopic picture of the sample of interest.

CONCLUSION

High resolution synchrotron infrared spectromicroscopy has potential for the direct facile and rapid comparative identification of writing inks. The technique can be used for the direct analyses of inks on paper without mechanically damaging the ink and paper or having to chemically extract or separate the ink. This method should be useful in other areas of studying ink, such as both qualitative and quantitative analysis of the ink components, verification of the identical nature of several inks, and the relative determination of the age of the ink.

This work was supported under the Center for Science and Engineering Education (CSEE) at the Lawrence Berkeley National Laboratory with support from the Director, Office of Science, Office of Basic Energy Sciences, Materials Science Division, the Office of Science Education, and the Special Technologies Program, of the U. S. Department of Energy under Contract Number DE-AC03-76SF00098.

Principal investigator: Dale Perry, Lawrence Berkeley National Laboratory, Phone: (510) 486-4819, Fax: (510) 486-5799, email: DLPerry@lbl.gov

X-ray Magnetic Linear Dichroism of Fe-Ni Alloys on Cu(111)

T.F. Johnson,[*] Y. Sato,[*] S. Chiang,[*] M. Hochstrasser, [#] J.G. Tobin[#], J.A. Giacomo,[*]
J.D. Shine,[*] X.D. Zhu,[*] D.P. Land,[**] D.A. Arena,[♦] S.A. Morton,[♣] G.D. Waddill[♣]
*Dept. of Physics, University of California, Davis
**Dept. Of Chemistry, University of California, Davis
#Lawrence Livermore National Laboratory, Livermore
♣University of Missouri, Rolla
♦Brookhaven National Laboratory, Upton, NY

INTRODUCTION

We are studying layer-by-layer synthesis of ultra-thin metal films by controlling at the monolayer level the composition and structure of these films, including the interfacial region. We have prepared Fe_xNi_{1-x} multilayers using simultaneous evaporation of pure Fe and Ni on Cu(111) in order to better understand the Giant Magnetoresistance (GMR) effect in FeNi/Cu systems that are relevant to magnetic disk drive heads. Using Undulator Beamline 7.0 and the Spin Spectroscopy Facility (7.0.1.2) at the ALS, we have measured X-ray Magnetic Linear Dichroism (XMLD) signals for twenty three different thin Fe-Ni alloys films on Cu(111) for different thicknesses and with Fe concentration ranging from 9% to 84%. X-ray Photoelectron Spectroscopy (XPS) with 1250 eV photon energy was utilized to determine both thickness and elemental composition. The Fe3p and Ni3p lines were measured for magnetization up and down, and the difference is the XMLD signal. Our XMLD spectra clearly indicate that samples of specific thicknesses and Fe concentrations are ferromagnetic. XMLD has previously been used to characterize Fe_xNi_{1-x} alloy fcc multilayers on Cu(100)[1].

RESULTS

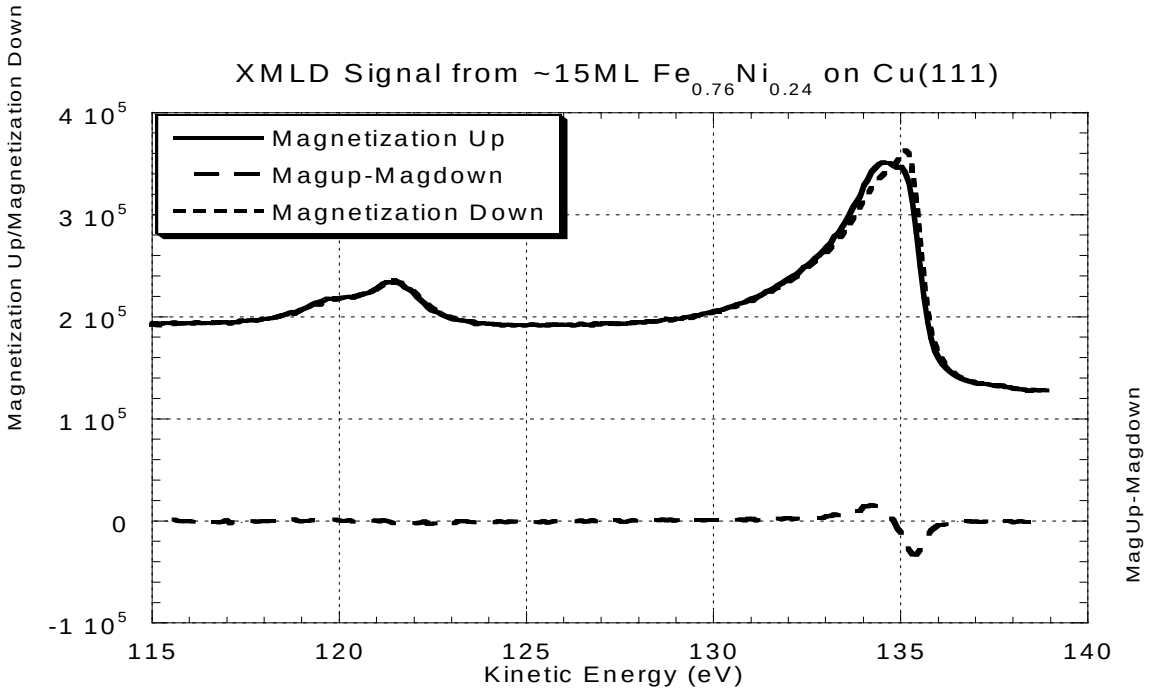

Figure 1. XMLD date from Fe-Ni thin film, 15ML thick, on Cu(111). Top of figures shows the signal for both magnetizations up and down. Bottom of figure shows difference, which is proportional to the dichroism.

Fig. 1 shows the XMLD effect for Fe concentration of 0.76 and thickness of 14ML. The upper panel clearly shows that the XPS data are different depending on the orientation of the applied field relative to the sample. The lower panel shows the difference between the two spectra in the upper panel and exhibits the dichroism effect. We have also measured the dichroism signal from both the Fe and the Ni peaks, which allows for calculation of the asymmetry.

The asymmetry is defined as, $\frac{\text{MagUp - MagDown}}{\text{MagUp + MagDown}}$, as measured from the XMLD signal.

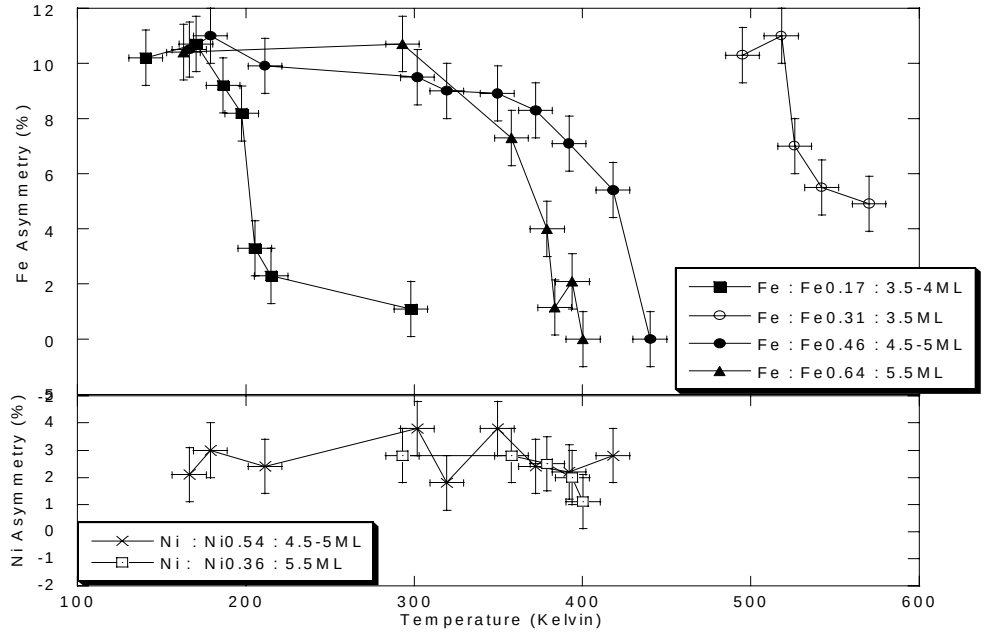

Figure 2. Fe and Ni asymmetry as a function of temperature for four Fe concentrations with film thicknesses near 5ML**.**

Figure 2 shows the asymmetry as a function of temperature for films with four different Fe concentrations and two different Ni concentrations, all ~5ML thick. The Fe data appear to fit the predictions from mean field theory, and preliminary attempts at mean field fits have had limited success. With increasing Fe concentration, the Curie temperature, where the asymmetry disappears, increases until x≈0.6, (near the Invar transition point) and then decreases.

Fig. 3 shows the total weighted asymmetry, $A_{T,}$ which is computed by performing a weighted sum of elemental asymmetries to obtain[2],

$$A_T=xA_{Fe}+(1-x)A_{Ni,},$$

with A_{Fe} and A_{Ni} being the asymmetries measured from the XMLD spectra for Fe and Ni respectively. Note that A_T also shows a magnetic instability near x=0.65. The data also support similar results by Schumann *et al* for FeNi on Cu(001). We observe that as the Fe concentration increases, we observe A_T to have an initial value of about 2%, which then monotonically increases to a maximum of about 8.5% at the Invar transition concentration. For Fe concentrations greater than x=0.65, the weighted asymmetry is quenched. As the system goes through the quenching transition, it goes from a highly aligned, high spin state to an admixture

that includes a low spin state for the Fe. For Fe on CuAu(100) multilayers, Keavney *et al*[3] also found high Fe asymmetry for Fe concentration less than or equal to 60%.

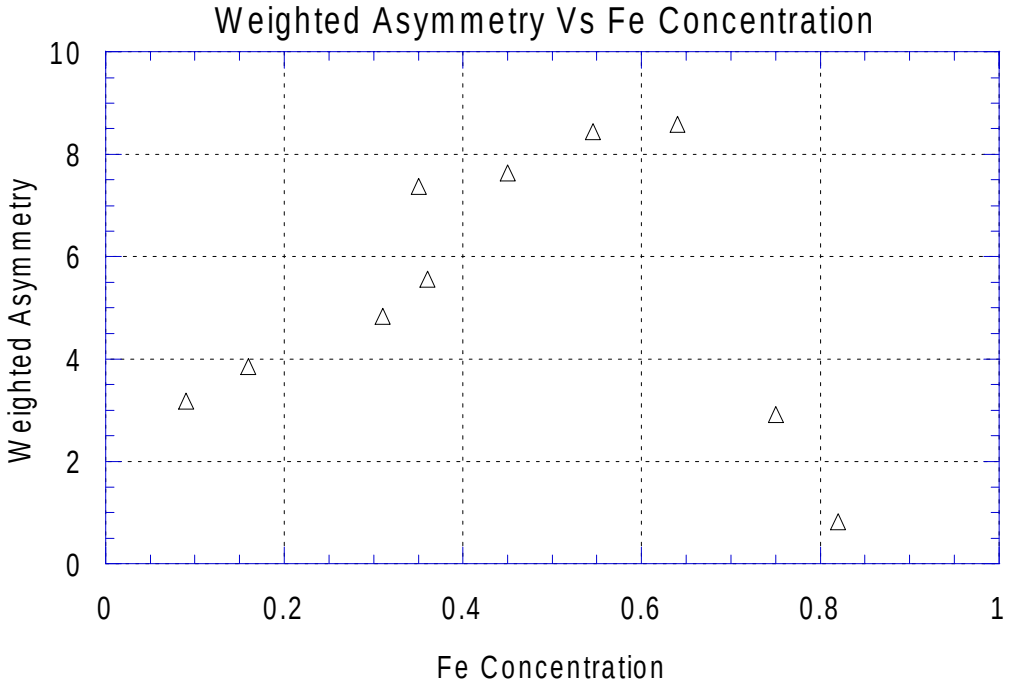

Fig. 3 Total weighted asymmetry of FeNi alloy as a function of Fe concentration for film thicknesses near 5 ML

Work is progress to compare the data in Figure 3 with previously published SQUID measurements[4] for FeNi films on Cu(111) in order to perform an absolute calibration of the XMLD signal.

REFERENCES

1. F. O. Schumann, R. F. Willis, K. G. Goodman, J. G. Tobin, Phys. Rev. Lett., **79**, 5166 (1997).
2. F. O. Schumann, R. F. Willis, J. G. Tobin, J. Vac. Sci. Tech. A **18**,1259 (2000).
3. D. J. Keavney, D. F. Storm, J. W. Freeland, I. L. Grigorov, J. C. Walker Phys. Rev. Lett., **74**, 4531 (1995).
4. J. W. Freeland, I. L. Grigorov, and J. C. Walker, Phys. Rev. B **57**, 80 (1998).

This work was supported by the Campus Laboratory Collaboration Program of the University of California Office of the President and was performed under the auspices of the U.S Department of Energy by Lawrence Livermore National Laboratory under contract no. W-7405-Eng-48. Experiments were carried out at the Spectromicroscopy Facility (Beamline 7.0) at the Advanced Light Source, built and supported by the Office of Basic Energy Sciences, U.S. Department of Energy.

Principal investigator: Shirley Chiang, Department of Physics, University of California, Davis, CA 95616-8677. Email: chiang@physics.ucdavis.edu. Telephone: 530-752-8538